Journal of
Food Chemistry & Nanotechnology

https://doi.org/10.17756/jfcn.2026-222

Research Article

Open Access

Sustainable Chitosan Groundnut Shell Hydrogel Beads for Adsorption/Desorption of Acid Black 172 Dye from Food Industry Wastewater

Asma Ashraf[1], Joydeep Dutta[1*], Arun Karnwal[2], Gaurav Kumar[3], Natalia Nesterova[4], George Kyzas[4], Ajendra Kumar[5] and Suhel Mehandi[6*]

[1]*Department of Zoology, School of Bioengineering and Biosciences, Lovely Professional University, Punjab, India*
[2]*Department of Microbiology, Graphic Era (Deemed to be University), Dehradun, Uttarakhand, India*
[3]*Amity Institute of Microbial Technology, Amity University, Rajasthan, India*
[4]*Hephaestus Laboratory, Faculty of Sciences, School of Chemistry, Democritus University of Thrace, Kavala, Greece*
[5]*Department of Mathematics and Statistics, Gurukula Kangri (Deemed to be University), Haridwar, Uttarakhand, India*
[6]*Department of Genetics and Plant Breeding, School of Agriculture, Lovely Professional University, Punjab, India*

***Correspondence to:**
Joydeep Dutta
Department of Zoology,
School of Bioengineering and Biosciences,
Lovely Professional University,
Punjab, India.
E-mail: joydeep.dutta@lpu.co.in

Suhel Mehandi
Department of Genetics and Plant Breeding,
School of Agriculture,
Lovely Professional University,
Punjab, India.
E-mail: suhel.26963@lpu.co.in

Received: January 09, 2026
Accepted: February 02, 2026
Published: February 06, 2026

Citation: Ashraf A, Dutta J, Karnwal A, Kumar G, Nesterova N, et al. 2026. Sustainable Chitosan Groundnut Shell Hydrogel Beads for Adsorption/Desorption of Acid Black 172 Dye from Food Industry Wastewater. *J Food Chem Nanotechnol* 12(1): 7-16.

Copyright: © 2026 Ashraf et al. This is an Open Access article distributed under the terms of the Creative Commons Attribution 4.0 International License (CCBY) (http://creativecommons.org/licenses/by/4.0/) which permits commercial use, including reproduction, adaptation, and distribution of the article provided the original author and source are credited.

Published by United Scientific Group

Abstract

The efficiency of low-cost, eco-friendly chitosan groundnut (*Arachis hypogaea*) shell powder (Ch-GNSP) composite beads were evaluated for the removal of Acid Black 172 (AB-172) dye. The composite was developed by integrating food-grade chitosan with agro-industrial groundnut shell waste, promoting sustainable biomass valorization for food-processing wastewater management. Parameters such as initial dye concentration, pH, contact time and adsorbent's dosage were evaluated in the batch adsorption experiments. The maximum removal (89%) was observed at pH 2, with an equilibrium attained at 60 min. The adsorption mechanism followed pseudo-second-order kinetics (R^2 = 0.994), signifying chemisorption. The data were most accurately represented by the Langmuir isotherm model (R^2 = 0.95), indicating monolayer adsorption with a calculated maximum adsorption capacity (q_m) of 53.30 mg/g (R^L = 0.2855). The separation factor confirmed that the adsorption process was favorable. Desorption of the dye was observed during the experiments for all initial concentrations within the 30 - 180 min interval. At 5 mg/L, desorption increased markedly from 21.9% to 85.3%, representing the highest recovery efficiency among the tested values. The enhanced adsorption performance is attributed to the functional amino groups of chitosan and the porous structural framework of the composite matrix, which provide abundant active binding sites. These results demonstrate that Ch-GNSP beads are effective for anionic dye removal under acidic conditions and hold promise as a sustainable food-compatible adsorbent for wastewater treatment applications, offering a practical solution for the removal of dyes generated by food-processing and related industries with good reusability potential.

Keywords

Adsorption, Beads, Chitosan, Groundnut shell powder, Metal complex dyes

Introduction

A clean environment is important for the survival of both aquatic and terrestrial (emerging contaminants (ECs)) biota. However, rapid growth in industrialization, household activities and agriculture has led to significant contamination in the aquatic ecosystems. Industries such as cosmetics, leather, paper, pharmaceuticals, and food release substantial quantities of effluents containing dyes into the water bodies annually [1]. Among various dyes used in a number of industries, azo dyes and their products are considered to be non-biodegradable, persistent and recalcitrant [2]. The release of untreated industrial dyes is a major

environmental concern as it contains hazardous intermediates that pose significant health risks to humans and ecosystem stability. The direct discharge of dyes is prone to precipitate on the water surface, thereby increasing turbidity and diminishing the aesthetic water quality and also negatively impacting microflora and both aquatic and terrestrial biological communities [3].

At present, several techniques and approaches have been widely developed to reduce the deleterious impact of dyes in wastewater, which include ion exchange, chemical coagulation-flocculation [4, 5], oxidation, chemical precipitation [5], photocatalytic degradation, ultrafiltration, membrane filtration [6] and nanofiltration [7]. These techniques have some notable limitations, including heightened demands for reagents and energy, reduced selectivity, considerable operational costs, incomplete removal of dye, energy necessity, high reagents and secondary wastes cost generation that are difficult to dispose of [8, 9]. Recent studies emphasize membrane technologies and advanced oxidation processes (AOPs) as a primary method for removing ECs.

Nevertheless, AOPs face limitations due to operational expenses and complex procedures, hindering their large-scale use [10]. Membrane technology, while promising, suffers from cost issues, and the management of brine poses both economic and environmental challenges [11]. Among all these techniques Adsorption process is the widely used technique due to its simplicity, sustainability, high efficacy and relatively cost-effective process. Due to the high sorption capacity and reduced contact time, the process is highly effective for large-scale removal applications [12]. It also has various benefits over conventional methods, such as reducing the generation of chemical sludge and undesirable by-products, the potential of metal recovery and regeneration of adsorbents [13]. Beyond their extensive use in leather and textile manufacturing industries, these dyes are also applied in food-processing units, sugar refining industries and food packaging inks. When effluents from those sectors are inadequately treated, dye-laden water waste can enter aquatic systems, raising concerns related to contamination of environment and safety for food. In food-processing environments, wash waters from colorant handling, beverage production lines, confectionery processing, and packaging operations may contain residual dye molecules that require careful treatment prior to discharge. The presence of persistent azo dyes in such effluents raises concerns not only about environmental contamination but also about regulatory compliance and indirect food-chain exposure risks. Therefore, sustainable and food-compatible wastewater treatment strategies are critically important for the food sector. The presence of chromium-containing dyes in food related effluents is a serious concern due to their bioaccumulative and toxic nature. Therefore, the development of biodegradable, food grade compatible adsorbents such as chitosan-based composites is highly relevant for sustainable treatment of food industry wastewater [13].

In recent years, low-cost adsorbents from agricultural and plant residues have gained attention for water pollutant removal. Among them, chitosan-rich in hydroxyl and amino groups stands out for its ability to efficiently eliminate diverse organic and inorganic contaminants, including metal-complex dyes. A naturally derived, non-toxic biopolymer that has been extensively used in food-grade applications such as edible coatings, food-packaging materials and the removal of contaminants from food-related systems [14]. Its recognition as a generally regarded as safe biopolymer further enhances its suitability for applications associated with food-processing wastewater systems, where material safety and biodegradability are essential considerations. Though effective, its practical use is limited by poor mechanical strength [14], low porosity [15] and acid instability [16]. Chitosan exhibits poor solubility at neutral pH due to the presence of both intramolecular and intermolecular hydrogen bonding. Moreover, its low antioxidant activity can be attributed to the absence of an H atom. It is rigid, has high hydrophilicity and has a fragile structure [17]. The hydroxyl (-OH) and amino ($-NH_2$) groups in chitosan function as the key factors that influence its antioxidant capabilities; nonetheless, their dissociation could lead to substantial complications owing to the semi-crystalline nature of chitosan and the formation of strong hydrogen bonds [18]. To improve its mechanical strength, a number of other materials have been incorporated into the chitosan matrix to make a chitosan composite bead to improve its efficiency for adsorption in aquatic biota [19].

The current research reveals the application of GNSP as an unconventional, economically viable adsorbent for the removal of AB-172 (molecular weight (MW) = 993.7 g/mol and λ_{max} = 597 nm) in aqueous phase. The AB-172 structure is presented in figure 1, a metal complex anionic azo dye which was selected for this study because it is a widely used persistent anionic azo dye known for its toxicity, carcinogenicity, and recalcitrant behavior, making it an ideal pollutant of water [20, 21]. Moreover, AB-172 having chromium in its

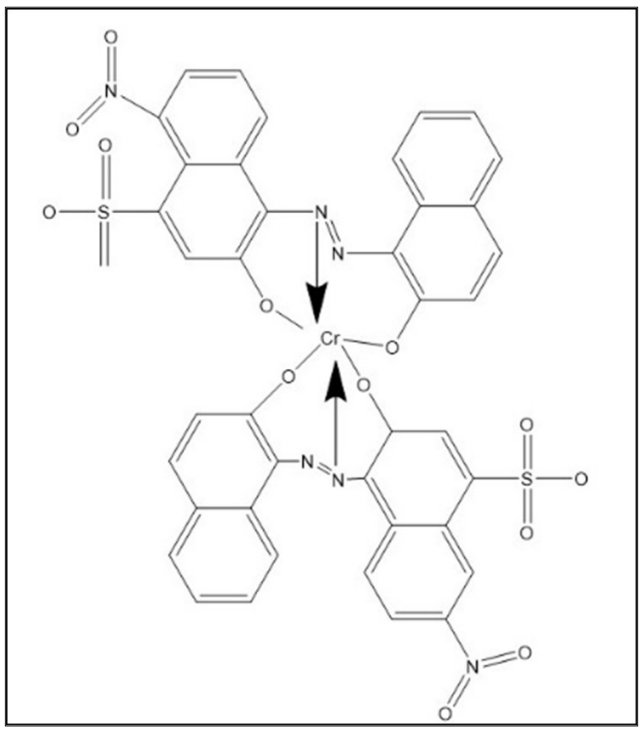


Figure 1: Structural composition of AB-172.

structure showing anionic metal complex dyes which is widely used in textile and tanning industry and its discharge into environment cause more serious problems in living biota like carcinogenic [22], and may rise in the trophic level through food chain and can also cause numerous pathophysiological defects in humans [23]. Chitosan's protonable -NH_2/-OH groups interact favorably with anionic via electrostatic attraction and hydrogen bonding, giving chitosan-based adsorbents strong removal potential [24]. Moreover, incorporating GN/peanut supplies low-cost, porosity and lignocellulosic binding sites that synergize with chitosan to increase surface area and mechanical stability of beads [25] a combination that has not been extensively explored to date.

GNSP is rich in lignin, has slow degradation in the natural environment and is widely used to absorb heavy metals and dyes [26]. As an abundant by-product generated during groundnut processing in the food and oil industries, its valorization into functional adsorbent materials supports circular bioeconomy principles by converting low-value biomass waste into high-value environmental remediation materials. The adsorption of bromophenol blue was achieved onto groundnut shell derived activated charcoal at a lower pH, which defines an electrostatic force of attraction generated due to opposite charges [27].

It is a natural absorbent and has better separation efficiency than other adsorbents. It is an eco-friendly bio-adsorbent, with a non-toxic nature, highly cost-effective and of low commercial value. In order to reduce disposal costs and expand its use for the removal of waste, groundnut shell is often used [28]. The study was undertaken to combine Ch-GNSP to form composite hydrogel beads, as the resulting material may offer more active binding sites and a synergistic effect, thereby enhancing the removal efficiency of heavy metals and dyes from water. The incorporation of GNSP, a readily available agro-industrial by product, improves the overall sustainability of the material by transforming waste biomass into a useful adsorbent which in turn will support economic concepts and make such materials suitable for treating wastewater generated from food processing industries [19].

Batch adsorption experiments were systematically examined to investigate the impact of some important factors, including dye concentration (initial), reaction time, pH and adsorbent dosage. The adsorption dynamics were assessed by applying both pseudo-first and second-order kinetic modelling to the experimental data. Furthermore, the adsorption isotherm data were thoroughly analyzed using the Langmuir and the Freundlich equilibrium models to determine the adsorption capacity and characterize the adsorption mechanism.

Materials and Methods

Chitosan (high MW: 1,500,000 g/mol avg), with (85% deacetylation degree) and sodium hydroxide pellets (NaOH) were purchased from Hi-Media Laboratories Pvt. Ltd. (Mumbai, India). Glutaraldehyde (25 wt.% aqueous solution) and acetic acid were purchased from Sigma Aldrich India. AB-172 was purchased from the local dye market and was used without undergoing any further purification.

Adsorbent's preparation

Ch-GNSP were taken in the ratio 1:1 (w/w), respectively, for the preparation of Ch-GNSP beads. Double-distilled water was used to rinse the wet beads to remove any unreacted cross-linker, and they were kept for drying in a hot air oven at 50 °C for about an hour. The beads, after drying, were stored in airtight packets under ambient conditions until further use [19].

Determination of pH at the point of zero charge (pH_{PZC})

The pH_{PZC} is characterized by the pH at which the surface of the adsorbent carries zero electric charge. The surface of the composite material tends to develop a negative charge if the pH is above the pH_{PZC} and a positive charge if it dips below pH_{PZC}. Ch-GNSP beads (50 mg) were added to an aliquot of 0.1 M sodium chloride. The pH of the solution was adjusted within the range of 4 - 10, using 0.1 M hydrochloric acid (HCL) and 0.1 M NaOH. The pH (initial) of the solutions was recorded, and the solutions were kept for shaking at 150 rpm for 24 h at an ambient temperature. The final reading was noted after 24 h [29]. The final pH of the solutions was noted, which was further analyzed as per the given equation:

$$\Delta pH = Initial\ pH - Final\ pH$$

Adsorption experiments

Batch adsorption experiment studies were performed to investigate the removal efficiency of AB-172 using the composited beads. Dye concentration solutions (5, 10, 15, 20 mg/L) were taken for the study. The adsorption experiment was carried out at ambient temperature (30 ± 2 °C) in Erlenmeyer flasks using various concentrations of the dye solution and adsorbent dosages (25, 50, and 100 mg/L). The pH was adjusted with either 1 M HCl or 1 M NaOH. The mixtures were continuously agitated at 160 rpm. The residual dye concentrations were analyzed at fixed time using an ultraviolet-visible (UV-Vis) spectrophotometer (λ = 597 nm) until equilibrium was achieved.

The amount of adsorbed dye was calculated by using the subsequent equation:

$$\frac{C_i - C_e}{C_0} \times 100\% \quad (1)$$

Where, C_i (mg/L) is the initial concentration, C_e (mg/L) is the final concentration and C_0 is the total concentration of AB-172 solution.

Desorption studies of Ch-GNSP beads

The release of AB-172 in aqueous solutions by the dye-loaded Ch-GNSP beads was investigated. Desorption involves breaking the interactions between the dye molecules and the chitosan surface. As reported by Liu et al. [30], 1 M NaOH was used as a strong alkali because it resulted in the deprotonation of amino groups on chitosan, reducing electrostatic attraction.

After the adsorption cycle, the dye-loaded Ch-GNSP beads are washed with distilled water to remove unbound dye. The beads were then soaked in a 50 mL NaOH solution (1

M concentration) using Erlenmeyer flasks at pH 2, as the adsorption efficiency was significantly higher in comparison to the other tested values. Hence, pH 2 was taken for desorption studies. The mixture was then agitated for 180 min at 150 rpm and at 30 ± 2 °C temperature. A 5 mL sample was taken every 30 min up to 180 min, and the concentration of AB-172 was noted using a UV-Vis spectrophotometer at 597 nm. The equation determined the desorption efficacy as:

$$\text{Desorption}\% = \frac{C_e}{C_0} \times 100\% \quad (2)$$

Where, Ce is the equilibrium concentration and C_0 is the dye adsorbed.

Results and Discussion

Adsorption evaluations

The influence of pH

The pH plays a crucial role in adsorption processes, influencing various aspects of the adsorption behavior, especially the surface charge of the dye and the adsorbent molecule. The pH significantly governs the adsorption behavior of chitosan-adsorbent molecules due to its effect on the protonation states of functional groups and charge of the surface material [24, 31-33]. The impact of solution pH on the adsorption of AB-172 by Ch-GNSP beads was initially analyzed from (pH 1 - 8) to identify the optimum condition for AB-172 uptake. The adsorption capacity of Ch-GNSP beads was found to be highest at lower pH values (1 - 4) and gradually decreased with increasing pH from 3 to 8. This behavior can be attributed to the protonation and deprotonation of chitosan's amino group [31, 32]. As seen in figure 2, the dye removal efficiency was notably higher in acidic conditions and progressively decreased as the pH increased. The results indicate a distinct decline with an increase in pH.

Maximum adsorption efficiency of 89% was observed at pH 2, which gradually declined to 64% and 52% at pH 3 and 4, respectively. The effectiveness of the composite under strongly acidic conditions is particularly relevant for certain food-processing effluents, where acidic cleaning streams and dye-containing wash waters are frequently encountered. This observation aligns with the typical behavior of chitosan adsorbent under acidic conditions. The amino groups ($-NH_2$) at lower pH values present in the chitosan matrix become protonated to form ammonia group ($-NH3^+$), resulting in a positively charged surface. This enhances the electrostatic force between the Ch-GNSP beads and the anionic sulfonate groups present in the AB-172 molecules. With the increase in pH, the amino group protonation decreases, leading to a reduced surface charge and diminished electrostatic interactions with the anionic dye species [34]. pH-sensitive Ch/itaconic acid/methacrylic acid hydrogel effectively eliminated colour index (C.I.) acid orange, C.I. basic red, and C.I. basic blue 9. Electrostatic interaction between cation or anion in the dye molecule and carboxyl (–COOH) or amino group ($-NH_2$) in the hydrogel plays a crucial role in azo dye removal [35]. At high pH, chitosan layers can contract and become more elastic due to the polymer's insolubility [36]. This change in physical properties can further affect the accessibility of adsorption sites and the overall efficacy of adsorption. Chitosan's elasticity in general tends to increase at lower pH levels [37]. The PZC was found to be 9. Above the value of PZC, the surface of the beads acquires increasingly negative charge, whereas below the PZC, the surface is positively charged below the PZC because the amino groups on chitosan become protonated to $-NH_3^+$ [38] through interactions with H^+ ions, leading to electrostatic attraction with the anionic azo dye (AB-172) [39].

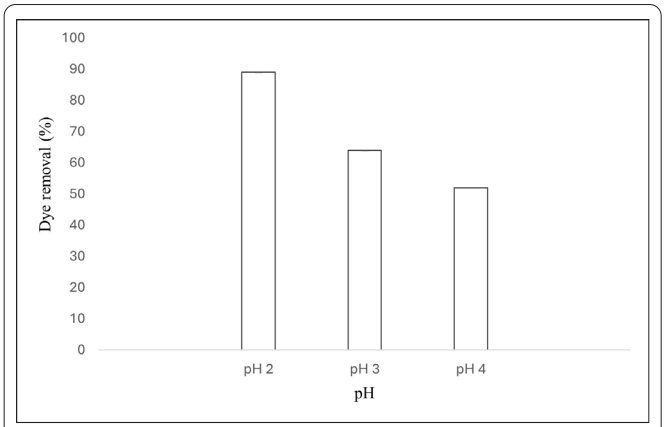


Figure 2: Influence of pH on AB-172 dye onto Ch-GNSP beads.

Effect of initial dye concentration

The adsorption performance of AB-172 onto Ch-GNSP beads was conducted by increasing the concentration from 5 - 20 mg/L. The maximum dye removal achieved in a concentration of 5 mg/L was 89%. The adsorption efficiency decreased with an increase in initial dye concentration. The trend could be attributed to the presence of the cationic charged adsorbent surface, resulting in the electrostatic interaction with the anionic AB-172 dye present in the aqueous phase [40]. The fourier transform infrared spectroscopy spectra of Ch-GNSP beads before adsorption reveal that amino and hydroxyl groups on the composite exhibit a strong affinity for anionic (AB-172), acting as active adsorption sites. After adsorption, shifts in O–H, N–H, and C=O peaks and the appearance of new aromatic bands confirm strong interactions between the dye and the Ch–GNSP composite. The results indicate hydrogen bonding and electrostatic interactions as the primary adsorption mechanisms [41]. Consequently, the molecules of dye progressively interact with these sites until saturation is attained [19].

The inverse correlation between the removal efficiency and initial dye concentration is attributed to the finite number of adsorption sites available at low concentrations. A 4.49% decrease was seen from concentration 5 to 10 mg/L, a more substantial decline of 13.7% occurred from 10 to 15 mg/L and a minor reduction of approximately 1.81% was seen from 15 to 20 mg/L (Figure 3). Such behavior can be ascribed to the ratio of dye to adsorbent concentration; low concentrations correspond to smaller dye molecules relative to available adsorption sites, while at elevated concentrations the reverse is true, inhibiting adsorption. Moreover, with an increase in initial dye concentration, the adsorbent capacity increases respectively, attributed to the gradient mass transfer potential with respect to increased initial concentration. Initial solute

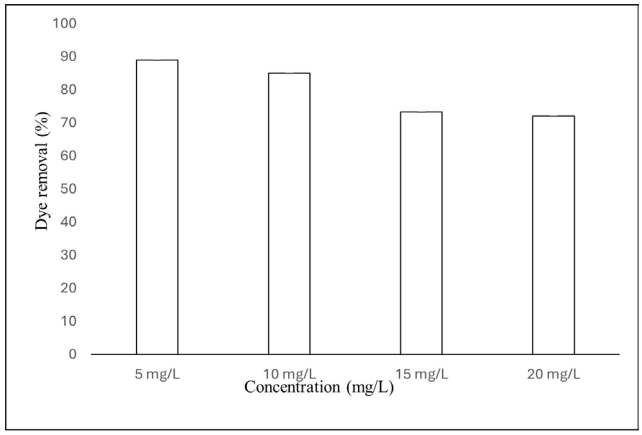


Figure 3: Effect of initial concentration on AB-172 removal.

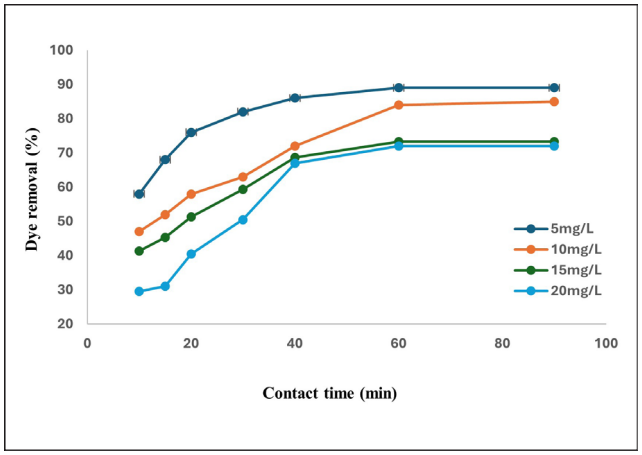


Figure 4: Influence of contact time on AB-172 dye onto Ch-GNSP beads.

concentration serves as a key driving force in the process, facilitating mass transfer and diffusion gradient from the solution (with an increased dye amount) to the adsorbents' available sites [42, 43]. The availability of active sites for dye molecules could be significantly high at low concentrations, facilitating prompt interactions and removal from solution almost instantaneously by the adsorbent [44]. As the solution concentration increases, as well as the bound material shows a similar trend, it can be inferred that at low dye concentration, the surface area of the adsorbent remains considerable, thus facilitating a significant number of binding sites of adsorption. As a result, the ions (in context, dye molecules) can interact with the adsorbent surface. When the concentration is increased, the availability of the adsorption sites is restricted, which may lead to the reduction of the contaminant's removal percentage. At higher concentrations, the driving force increases respectively [45].

Contact time and adsorption dynamics

AB-172 adsorption process onto Ch-GNSP beads was evaluated at varying initial dye concentrations (5, 10, 15, and 20 mg/L) over a period of 90 min. A rapid increase in dye removal was observed during the first 30 min for all concentrations, signifying the presence of numerous active sites on the surface adsorbent and a strong electrostatic force of attraction between the anionic dye and the protonated amino groups of chitosan [46]. At 5 mg/L, dye removal increased from 58 to 82% within the first 30 min, eventually reaching 89% at 60 min, after which no further increase was observed, indicating equilibrium. A uniform trend was observed for 10 mg/L, where adsorption rose from 47 to 84% in 60 min (Figure 4). For higher concentrations (15 and 20 mg/L) with maximum removal of 73.33 and 72%, respectively, at 60 min. The rate of dye removal was comparatively slower because of increased competition among dye molecules for available binding sites, but after some time, the available sites are subsequently bound by dye molecules, inducing a repulsive force between the bulk phase and adsorbent [47]. After 60 min, adsorption values plateaued for all concentrations, suggesting that equilibrium was attained. Thus, 60 min was identified as the equilibrium contact time for effective adsorption, and the results also confirm that lower initial concentrations favor faster and more efficient dye uptake due to better accessibility to active adsorption sites.

Effect of the adsorbent's dosage

The mass of adsorbent plays an important role in adsorption processes and can significantly affect the effectiveness and efficiency of the process. The increase in the dosage of the adsorbent is correlated with the overall performance and efficiency of the removal of the contaminant. An increase in the adsorbent dosage leads to an increase in the surface area available for the adsorption process [48]. The dose effect was studied in the range of 25, 50, and 100 mg. As shown in figure 5, with an increase in adsorbent dosage, the removal efficiency of AB-172 increased from 20 to 40% at a dose of 25 mg, 48 to 78% at 50 mg and 58 to 89% at 100 mg dosage. These findings corroborate earlier reports that an increased amount of adsorbent to achieve the same initial concentration removes all adsorbate, thereby inducing mass transfer limitations that result in saturation and a plateaued adsorption capacity [49]. The rise in efficiency continues until saturation is obtained, therefore, exhibiting a gradual decline or minor fluctuations. This can be attributed to the point at which the adsorbent dose becomes sufficient for maximum adsorption, resulting in equilibrium where the number of bound ions and the concentration of free ions remain unchanged despite adding more

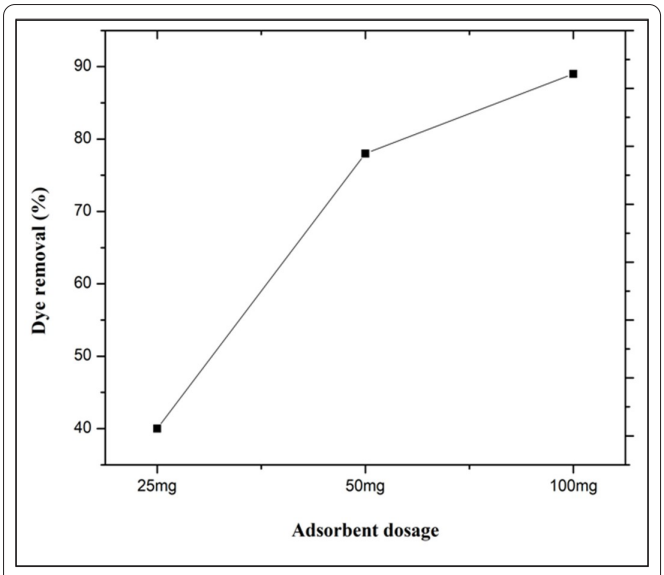


Figure 5: Role of adsorbent dosage on removal of AB-172.

adsorbent [50-52]. Based on the mass balance principle, the observed decrease in dye uptake per unit mass of adsorbent with increasing dosage is therefore expected. These findings indicate that dosage optimization is essential for scaling the process to industrial applications, particularly in food-processing wastewater systems where cost-efficiency and material utilization are critical. Dye uptake per mass unit decreases because the equilibrium dye concentration increases with an increasing adsorbent dose [53].

Adsorption isotherms

Adsorption isotherms define how molecules of dye are distributed and how they interact with the adsorbent surface at saturation. These isotherms define the interaction between adsorbate concentration and adsorption capacity at constant temperature. Various isotherms are available. However, for this study, two prominent isotherms were chosen: Langmuir and the Freundlich models, owing to their proven reliability and simplicity [54].

The data derived from various initial dye concentrations on the 1:1 Ch-GNSP beads were used to analyze the adsorption isotherm models. Four dye concentrations (5, 10, 15, 20 mg/L) were selected for the isotherm evaluation. The present analysis conducted a systematic examination of both the Langmuir and the Freundlich models. The application of adsorption isotherm models to experimental data facilitates the design of adsorption systems for practical applications [55].

Langmuir isotherm

The Langmuir isotherm [56] model (Figure 6) is formulated as

$$\frac{C_e}{q_e} = \frac{C_e}{q_m} + \frac{1}{K_L q_m} \quad (3)$$

Where, C_e (mg/L) is the initial dye concentration, q_e is the amount of the adsorbed dye, q_m is the maximum adsorption, and K_L (mg/L) is the Langmuir equilibrium constant.

R_L known as separation, is used to assess the favorability of the adsorption process. It is represented as:

$$R_L = \frac{1}{1 + K_L C_0} \quad (4)$$

Freundlich isotherm

The Freundlich isotherm [57] model (Figure 7) favors heterogeneous adsorption on surfaces. It is a multilayer adsorption.

$$q_e = K_F C_e^{1/n} \quad (3)$$

Where, q_e is the amount of absorbate adsorbed, K_F is the Freundlich constant related to adsorption capacity, 1/n indicates the heterogeneity factor, and C_e is the equilibrium concentration of adsorbate.

According to the correlation coefficient presented in table 1, the analyzed data showed an excellent fit with the Langmuir isotherm, signifying monolayer adsorption upon a uniform surface [58]. The maximum adsorption capacity q_m (mg.g^{-1}) of the biosorbent beads was determined to be 53.304 mg·g^{-1} indicating that each gram of Ch-GNSP beads can adsorb up to 53.304 mg/g mg of AB-172 at saturation. The Langmuir constant, K_L = 0.035 mg^{-1}), further reflects a high adsorption affinity among the dye molecules and the interaction sites on the biosorbent surface. The calculated separation factor R_L = 0.28554, lying well within the favorable range of 0 to 1, confirms the favorable and spontaneous nature of the adsorption process. Moreover, the high correlation coefficient (R^2) = 0.95 indicates an excellent fit of the experimental data to the Langmuir isotherm model, suggesting that the adsorption mechanism is predominantly governed by homogeneous sur-

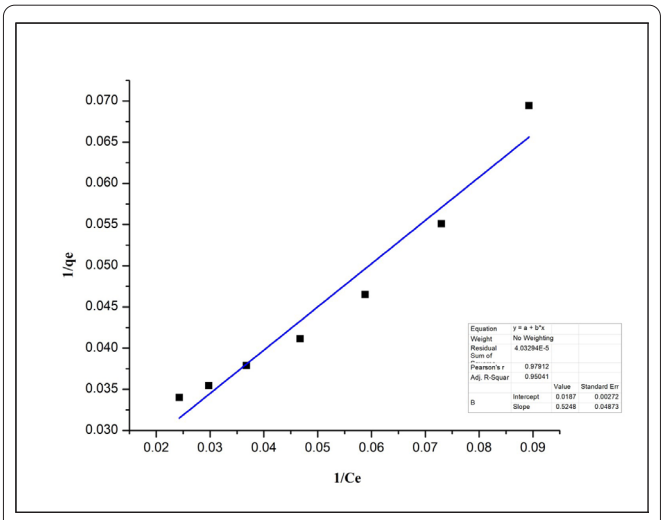


Figure 6: Langmuir isotherm modeling fit of AB-172 adsorption onto Ch-GNSP beads.

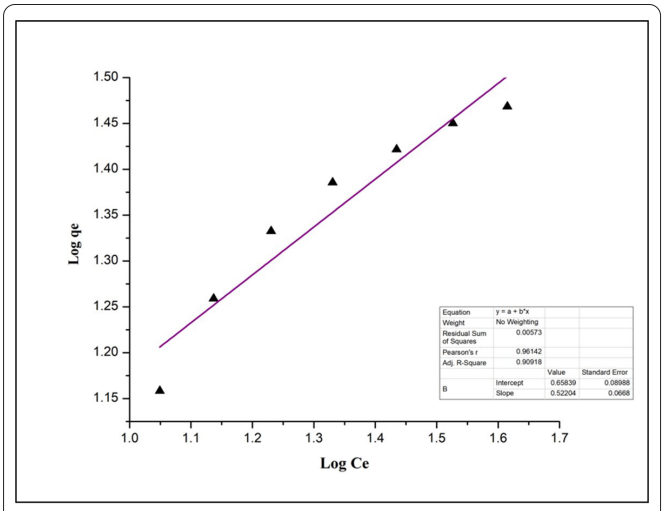


Figure 7: Freundlich isotherm modelling fit of AB-172 adsorption onto Ch-GNSP beads.

Table 1: Influence of isotherm models on the adsorption of AB-172.

Langmuir isotherm				Freundlich isotherm		
q_m (mg/g)	K_L (mg/L)	R_L	R^2	K_F (mg/g) (L/mg) (1/n)	n	R^2
53.304	0.035	0.28554	0.95	4.5539	1.9155	0.909

face binding with minimal interaction among adsorbed species. However, in the Freundlich isotherm, the constants (K_F = 4.553 mg/g and n = 1.9155) indicated favorable adsorption, as well as the value of n was greater than 1, suggesting a heterogeneous surface with good intensity of adsorption. However, the slightly lower R^2 = 0.909 compared to the Langmuir model points out that multilayer adsorption plays a smaller role, while monolayer adsorption is dominant.

Adsorption kinetic modelling

The kinetic behavior of the adsorption process involving the removal of AB-172 onto Ch-GNSP beads was assessed using pseudo-first and second order models in order to understand the adsorption mechanism and also the rate-controlling steps.

Pseudo-first-order kinetic modelling

The pseudo-first order kinetic modelling (Figure 8) suggests that the change of rate in the uptake of solute with the reaction time is directly proportional to the difference between the equilibrium adsorption capacity and the absorbed amount at time t [59]. The model was applied to experimental data, and the parameters were determined (Table 2).

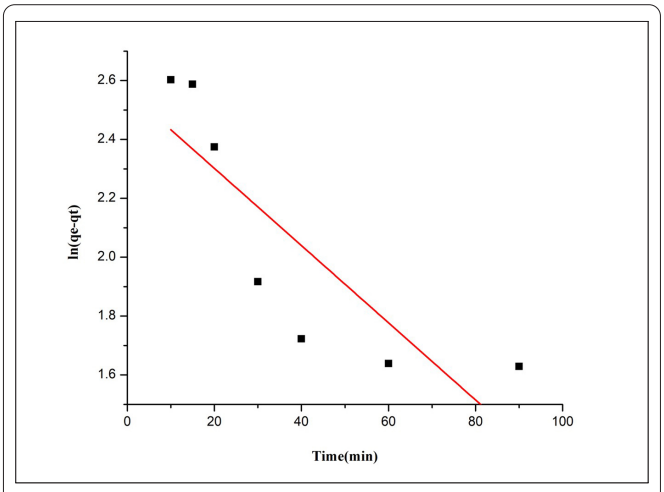


Figure 8: Pseudo first order modelling.

Table 2: Comparative evaluation and implications.

Parameter	Pseudo-first order	Pseudo-second order
Rate constant	0.01312 min^{-1}	0.00515 g/mg·min
R^2	0.664	0.994
q_e	12.99 mg/g	26.72 mg/g

Pseudo-second order kinetic modelling

The pseudo-second order (Figure 9) hypothesis indicates that the process of adsorption is mainly governed by chemisorption, including valence interactions from sharing and exchanging electrons between the adsorbate and the adsorbent [59]. The model was applied to examine the adsorption data, and the important factors were determined (Table 2).

Kinetic studies were analyzed for optimizing the operational conditions of dye AB-172 adsorption onto Ch-GNSP beads (Figure 8 and figure 9). The order of the adsorption and rate constants was fitted to pseudo-first order and pseudo-second-order models.

The pseudo-second-order model demonstrates a markedly higher coefficient of determination (R^2 = 0.994) compared to the value of 0.664, indicating an excellent correlation with the experimental data and strongly validating the appropriateness of this model (Table 2). Moreover, the equilibrium adsorption capacity (q_e, calc) (26.72 mg/g) was in close agreement with the experimental data (q_e, exp) at all initial dye concentrations, indicating that the adsorption process follows the pseudo-second-order kinetic model. This also suggests that boundary layer resistance is not the controlling factor, as the dye uptake is governed by pseudo-second-order kinetics [60]. On the other hand, the pseudo-first-order rate constant (K_L = 0.0312 min^{-1}) and the lower value (12.00 mg/g) showed a weaker correlation with the experimental data.

Desorption studies

Four different concentrations (5, 10, 15, and 20 mg/L) of AB-172 were evaluated. Desorption of the dye was observed during the experiment with an increasing trend and was noted for all the initial concentrations taken in the study, with the time interval of 30 - 180 min. At 5 mg/L, desorption (%) increased markedly from 21.9 to 85.3(Δ63.4; figure 10a), representing the highest recovery efficiency among tested values. At 10 mg/L, desorption % increased from 20.1 to 49.3 (Δ29.2%; figure 10b), while at 15 mg/L it rose from 15.2 to 43.5 (Δ28.3%; figure 10c). The lowest increase was observed at (20 mg/L from 12.6 to 32.3 (Δ19.7; figure 10d), respectively. It may also be observed that the desorption was quite high in dye concentrations 5 mg/L and 10 mg/L showing efficient removal of the adsorbed dye ions, followed by 15 mg/L and 20 mg/L dye concentrations. This indicates that lower initial dye concentrations lead to higher desorption. This trend can be due to the active sites' availability on the Ch-GNSP beads; at lower dye concentrations, the adsorbent sites are less saturated, facilitating higher desorption rates. This behavior aligns with findings in adsorption-desorption studies where increasing initial dye concentrations tends to decrease desorption efficiency due to the saturation of adsorption sites and more robust binding of the adsorbate to the adsorbent surface [31].

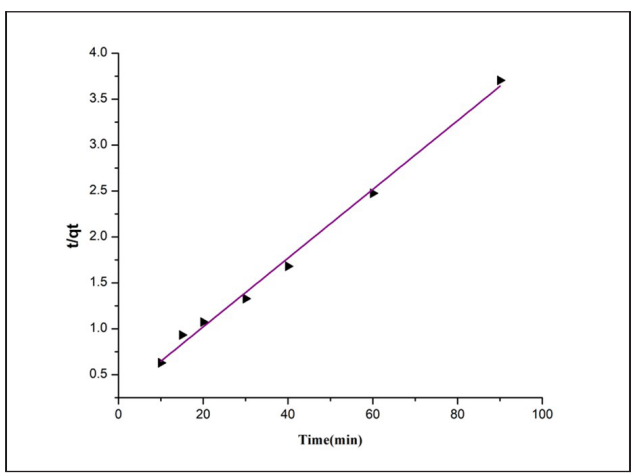


Figure 9: Pseudo second order modelling.

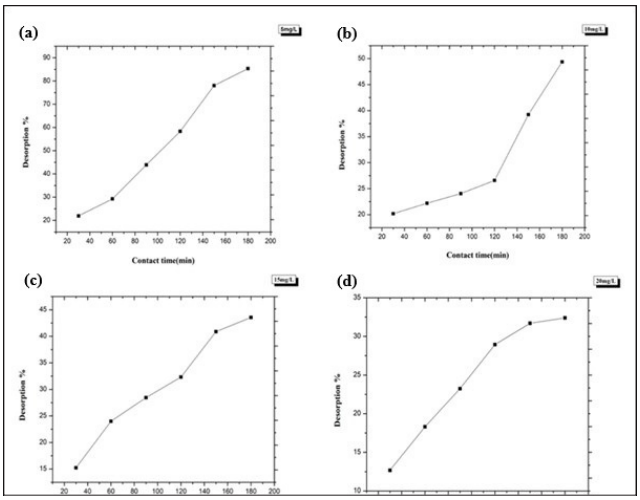


Figure 10: Desorption of AB-172 from Ch-GNSP beads at different initial dye concentrations: **(a)** 5 mg/L; **(b)** 10 mg/L; **(c)** 15 mg/L; and **(d)** 20 mg/L.

Mechanism driving desorption increase over time

The NaOH induced desorption mechanism is governed by the deprotonation of the amino group on the adsorbent surface, which results in the formation of negatively charged adsorption sites. The increase in desorption percentage over time is primarily driven by the gradual weakening of electrostatic affinity between functional groups of chitosan and anionic sites of dye molecules, and adsorbed ions are then separated from sites of adsorption, allowing dye molecules to be released back into the solution. However, prolonged contact time facilitates disruption of these. Desorption efficiency is enhanced, and the release of adsorbed ions also increases at high temperature due to the dissociation of adsorbate and adsorbent binding. Some studies examined the desorption efficacy of chitosan adsorbents and revealed that adjusting the pH level improved the desorption efficiency of adsorbents [61-63].

Conclusions

The research focused on examining how Ch-GNSP composite beads can be synthesized and utilized, showcasing their affordable capacity, environmentally safe, and impactful biosorbent for AB-172 dye extraction from water. In addition, the development of this composite material emphasizes the integration of a food-grade biopolymer (chitosan) with agro-industrial waste biomass, supporting sustainable material innovation within food-processing and related industrial wastewater systems. A set of batch adsorption experiments was carried out, systematically investigating the adsorption behaviors of the biosorbent by adjusting key operational factors like dye concentration (initial), reaction time, pH of the solution and adsorbent dose. Adsorption efficacy of the Ch-GNSP beads was determined to be significantly influenced by pH, with optimal dye removal (89%) attained at an acidic pH (pH 2), attributable to the increased availability of amino groups on chitosan, which augmented electrostatic interactions with the anionic dye molecules. This behavior highlights the functional role of protonated amino groups within the biopolymeric hydrogel network, which enhances dye–polymer interactions and supports its applicability in treating effluents generated from food colorant and food-processing industries. An inverse relationship between the outset of dye concentration and the extent of dye removed was noted, illustrating the saturation of accessible active sites at increased dye concentrations. Achieving optimal adsorption in 60 min confirmed the swift kinetics and the effective availability of the binding sites.

The pseudo-second-order model, based on kinetic modeling, stands out as providing the most precise depiction of the experimental data, highlighted by a more favorable coefficient of correlation (R^2 = 0.994) as opposed to the pseudo-first-order model (R^2 = 0.664). The notable alignment observed between the computed and observed equilibrium sorption capacities reinforced the pseudo-second order model's validity, signifying that chemisorption is likely the leading mechanism. Additionally, the significance of boundary layer resistance was assessed as negligible, implying that external mass transfer was not a constraining factor in the adsorption process. Research focusing on isotherms indicated that the adsorption equilibrium information demonstrated a closer match to the Langmuir model (R^2 = 0.95), reflecting monolayer adsorption on an even surface. The highest monolayer adsorption capacity (q_m) was ascertained to be 53.30 mg/g, and the dimensionless separation parameter (R_L = 0.2855) affirmed that the adsorption process was favorable and occurred spontaneously. The Freundlich model also demonstrated a reasonable fit, albeit with a lower correlation coefficient, suggesting that multilayer adsorption played a minimal role. These adsorption characteristics indicate the presence of well-distributed active sites within the composite hydrogel matrix, potentially attributed to micro- to nano-scale structural features that enhance surface functionality and adsorption efficiency.

Desorption studies highlighted the highest desorption percentage (85.3) at a lower concentration (5 mg/L) and decreased with increasing dye concentration. 32.2 desorption percentage was observed in 20 mg/L, suggesting that lower initial dye concentrations lead to higher desorption. The availability of active sites on the Ch-GNSP beads, at lower dye concentrations, results in the adsorbent sites being less saturated, facilitating higher desorption rates. Together, these outcomes validate that Ch-GNSP composite beads function as a highly competent and environmentally sustainable biosorbent for wastewater polluted with dye. From a food chemistry and sustainability perspective, the valorization of groundnut shell waste combined with a biodegradable, food-compatible polymer underscores the material's potential for eco-friendly wastewater management in food production and allied industries. The impressive removal efficiency, swift equilibrium attainment, strong alignment with kinetic and isotherm models, and the employment of inexpensive, renewable agricultural waste materials underscore the practical feasibility of this biosorbent for large-scale water treatment applications. Furthermore, the biodegradable nature and low toxicity profile of chitosan-based composites enhance their suitability for applications associated with food-related environments where safety and environmental compatibility are essential. Subsequent research endeavors may examine the regeneration and reuse of the beads, adsorption in continuous flow systems, and the removal of additional ECs to evaluate their practical utility

in environmental remediation further. Future studies should also focus on detailed nano-scale structural characterization, performance evaluation in real food-processing effluents, and scale-up feasibility to strengthen their applicability within sustainable food industry frameworks.

Acknowledgements

The author is grateful to the Lovely Professional University administration for providing the essential facilities required for conducting lab and field trials.

Conflict of Interest

None.

References

1. Yadav D, Rangabhashiyam S, Verma P, Singh P, Devi P, et al. 2021. Environmental and health impacts of contaminants of emerging concerns: recent treatment challenges and approaches. *Chemosphere* 272: 129492. https://doi.org/10.1016/j.chemosphere.2020.129492
2. Oladimeji TE, Oyedemi M, Emetere ME, Agboola O, Adeoye JB, et al. 2024. Review on the impact of heavy metals from industrial wastewater effluent and removal technologies. *Heliyon* 10(23): 1-30. https://doi.org/10.1016/j.heliyon.2024.e40370
3. Khan A, Nayarisseri A, Singh SK. 2025. Characterization and optimization of azo dyes degrading microbes isolated from textile effluent. *Sci Rep* 15: 1-23. https://doi.org/10.1038/s41598-025-95359-2
4. Verma AK. 2024. Bio-adsorbent for elimination of reactive dye from aqueous solution: kinetic and statistical modelling study. *Recent Innov Chem Eng* 18(3): 238-252. https://doi.org/10.2174/0124055204346559241007110823
5. Ross N, Tambwe K. 2024. Nanostructured Silver-iron-functionalized Titanium Dioxide Photo Electrocatalyst for Industrial Effluent Remediation. In Raju K, Makgopa K, Modibane KD, Lichtfouse E (eds) Nanoelectrocatalysts for Energy and Water Treatment. Environmental Chemistry for a Sustainable World. Springer, pp 439–460.
6. Binazadeh M, Rasouli J, Sabbaghi S, Mousavi SM, Hashemi SA, et al. 2023. An overview of photocatalytic membrane degradation development. *Materials* 16(9): 3526. https://doi.org/10.3390/ma16093526
7. Kumar A, Rana S, Dhiman P, Sharma P, Lai CW, et al. 2025. Recent progress in integration of photocatalysis and nanofiltration for advanced wastewater treatment. *Front Environ Sci Eng* 19: 1–24. https://doi.org/10.1007/s11783-025-2070-z
8. Binazadeh M, Li Z, Karimi IA. 2020. Optimization of biodegradation of long chain n-alkanes by Rhodococcus sp. Moj-3449 using response surface methodology. *Phys Chem Res* 8(1): 45–59. https://doi.org/10.22036/pcr.2019.204077.1682
9. Kusworo TD, Kumoro AC, Aryanti N, Hasbullah H, Chaesarifa DR, et al. 2023. Developing a robust photocatalytic and antifouling performance of PVDF membrane using spinel $NiFe_2O_4$/GO photocatalyst for efficient industrial dye wastewater treatment. *J Environ Chem Eng* 11(2): 109449. https://doi.org/10.1016/j.jece.2023.109449
10. Fernandes J, Ramísio PJ, Puga H. 2024. A comprehensive review on various phases of wastewater technologies: trends and future perspectives. *Eng* 5(4): 2633–2661. https://doi.org/10.3390/eng5040138
11. Verlicchi P. 2018. Hospital Wastewaters. Springer.
12. Nugraha MW, Kim S, Roddick F, Xie Z, Fan L. 2025. A review of the recent advancements in adsorption technology for removing antibiotics from hospital wastewater. *J Water Process Eng* 70: 106960. https://doi.org/10.1016/j.jwpe.2025.106960
13. Bayuo J, Rwiza MJ, Choi JW, Mtei KM, Hosseini-Bandegharaei A, et al. 2024. Adsorption and desorption processes of toxic heavy metals, regeneration and reusability of spent adsorbents: economic and environmental sustainability approach. *Adv Colloid Interface Sci* 329: 103196. https://doi.org/10.1016/j.cis.2024.103196
14. Ashraf A, Dutta J, Farooq A, Rafatullah M, Pal K, et al. 2024. Chitosan-based materials for heavy metal adsorption: recent advancements, challenges and limitations. *J Mol Struct* 1309: 138225. https://doi.org/10.1016/j.molstruc.2024.138225
15. Mathew SA, Arumainathan S. 2022. Crosslinked chitosan–gelatin biocompatible nanocomposite as a neuro drug carrier. *ACS Omega* 7(22): 18732–18744. https://doi.org/10.1021/acsomega.2c01443
16. Dotto G, Pinto L. 2011. Adsorption of food dyes acid blue 9 and food yellow 3 onto chitosan: stirring rate effect in kinetics and mechanism. *J Hazard Mater* 187(1-3): 164–170. https://doi.org/10.1016/j.jhazmat.2011.01.016
17. Begum S, Yuhana NY, Saleh NM, Kamarudin NH, Sulong AB. 2021. Review of chitosan composite as a heavy metal adsorbent: material preparation and properties. *Carbohydr Polym* 259: 117613. https://doi.org/10.1016/j.carbpol.2021.117613
18. Ivanova DG, Yaneva ZL. 2020. Antioxidant properties and redox-modulating activity of chitosan and its derivatives: biomaterials with application in cancer therapy. *BioRes Open Access* 9(1): 64–72. https://doi.org/10.1089/biores.2019.0028
19. Dutta J, Ashraf A, Mehmi S, Kumar A, Alodhayb A, et al. 2023. Synthesis and characterization of peanut hull modified chitosan beads. *Environ Sci Pollut Res* 30(39): 90721–90729. https://doi.org/10.1007/s11356-023-28787-0
20. Yang Y, Wang G, Wang B, Li Z, Jia X, et al. 2011. Biosorption of acid black 172 and congo red from aqueous solution by nonviable Penicillium YW 01: kinetic study, equilibrium isotherm and artificial neural network modeling. *Bioresour Technol* 102(2): 828–834. https://doi.org/10.1016/j.biortech.2010.08.125
21. Ciobanu G, Harja M, Rusu L, Mocanu AM, Luca C. 2014. Acid black 172 dye adsorption from aqueous solution by hydroxyapatite as low-cost adsorbent. *Korean J Chem Eng* 31(6): 1021–1027. https://doi.org/10.1007/s11814-014-0040-4
22. Bakshi A, Panigrahi AK. 2018. A comprehensive review on chromium induced alterations in fresh water fishes. *Toxicol Rep* 5: 440–447. https://doi.org/10.1016/j.toxrep.2018.03.007
23. Aksu Z, Balibek E. 2010. Effect of salinity on metal-complex dye biosorption by *Rhizopus arrhizus*. *J Environ Manage* 91(7): 1546–1555. https://doi.org/10.1016/j.jenvman.2010.02.026
24. Alves DCS, Healy B, Pinto LA, Cadaval TR, Breslin CB. 2021. Recent developments in chitosan-based adsorbents for the removal of pollutants from aqueous environments. *Molecules* 26(3): 594. https://doi.org/10.3390/molecules26030594
25. Almeida-Naranjo CE, Frutos M, Guerrero VH, Villamar-Ayala C. 2024. Characterization and performance of peanut shells in caffeine and triclosan removal in batch and fixed-bed column tests. *Molecules* 29(12): 2923. https://doi.org/10.3390/molecules29122923
26. Duc PA, Dharanipriya P, Velmurugan BK, Shanmugavadivu M. 2019. Groundnut shell-a beneficial bio-waste. *Biocatal Agric Biotechnol* 20: 101206. https://doi.org/10.1016/j.bcab.2019.101206
27. Raghunathan G, Rajagopal P, Chithra K. 2022. Arachis hypogaea shell–an approach towards waste utilization for cationic and anionic dye removal. *Clean Eng Technol* 6: 100385. https://doi.org/10.1016/j.clet.2021.100385
28. Muzakir MM, Joshua J. 2023. Kinetics and thermodynamics of sorption of methylene blue dye onto raw groundnut shell biosorbent. *J Environ Bioremediation Toxicol* 6(1): 1–7. https://doi.org/10.54987/jebat.v6i1.796
29. Çınar S, Dinçer A, Eser A, Aydemir T. 2023. Application of crosslinked chitosan-nanoclay composite beads for efficient removal of Ponceau S azo dye from aqueous medium. *Toxicol Rev* 42(3): 599–614. https://doi.org/10.1080/15569543.2023.2204367
30. Liu Y, Lang C, Ding Y, Sun S, Sun G. 2023. Chitosan with enhanced

deprotonation for accelerated thermosensitive gelation with β-glycerophosphate. *Eur Polym J* 196: 112229. https://doi.org/10.1016/j.eurpolymj.2023.112229

31. Ngah WW, Teong LC, Hanafiah MM. 2011. Adsorption of dyes and heavy metal ions by chitosan composites: a review. *Carbohydr Polym* 83(4): 1446–1456. https://doi.org/10.1016/j.carbpol.2010.11.004
32. Aranaz I, Alcántara AR, Civera MC, Arias C, Elorza B, et al. 2021. Chitosan: an overview of its properties and applications. *Polymers* 13(19): 3256. https://doi.org/10.3390/polym13193256
33. Aljawish A, Chevalot I, Jasniewski J, Scher J, Muniglia L. 2015. Enzymatic synthesis of chitosan derivatives and their potential applications. *J Mol Catal B Enzym* 112: 25–39. https://doi.org/10.1016/j.molcatb.2014.10.014
34. Rinaudo M. 2006. Chitin and chitosan: properties and applications. *Prog Poly Sci* 31(7): 603-632. https://doi.org/10.1016/j.progpolymsci.2006.06.001
35. Lučić-Škorić M, Stanojković LS, Milosavljević N, Krušić MK. 2018. Sorption of textile dyes from textile wastewater by chitosan-based hydrogel. *Tehnika* 73(1): 11–18. https://doi.org/10.5937/tehnika1801009L
36. Myllytie P, Salmi J, Laine J. 2009. The influence of pH on the adsorption and interaction of chitosan with cellulose. *BioResources* 4(4): 1647–1662. https://doi.org/10.15376/BIORES.4.4.1647-1662
37. Zhang S, Ji Y, He Y, Dong J, Li H, et al. 2024. Effect of environmental pH on the mechanics of chitin and chitosan: a single-molecule study. *Polymers* 16(7): 995. https://doi.org/10.3390/polym16070995
38. Elhady S, Bassyouni M, Elshikhiby MZ, Saleh MY, Elzahar MH. 2024. Optimization of anionic dye removal using cross-linked chitosan composite as eco-friendly bio-adsorbent. *Appl Water Sci* 14(7): 1-22. https://doi.org/10.1007/s13201-024-02210-6
39. Salama A, El-Sakhawy M. 2023. Synthesis and adsorption performance of functionalized chitosan and carboxyethylsilanetriol hybrids. *BMC Chem* 17(1): 1-9. https://doi.org/10.1186/s13065-023-00943-0
40. Strebel A, Behringer M, Hilbig H, Machner A, Helmreich B. 2024. Anionic azo dyes and their removal from textile wastewater through adsorption by various adsorbents: a critical review. *Front Environ Eng* 3: 1-17. https://doi.org/10.3389/fenve.2024.1347981
41. Kyomuhimbo HD, McHunu W, Arnold M, Feleni U, Haneklaus NH, et al. 2024. Synthesis and dye adsorption dynamics of chitosan–polyvinylpolypyrrolidone (PVPP) composite. *Polymers* 16(18): 2555. https://doi.org/10.3390/polym16182555
42. Seow TW, Lim CK. 2016. Removal of dye by adsorption: a review. *Int J Appl Eng Res* 11: 2675–2679.
43. Al-Ghouti MA, Al-Absi RS. 2020. Mechanistic understanding of the adsorption and thermodynamic aspects of cationic methylene blue dye onto cellulosic olive stones biomass from wastewater. *Sci Rep* 10(1): 1-18. https://doi.org/10.1038/s41598-020-72996-3
44. Silva CEF, da Gamadutt BMV, Gonçalves AHS, Medeiros JA, de Souza Abud AK. 2020. Basic-dye adsorption in albedo residue: effect of pH, contact time, temperature, dye concentration, biomass dosage, rotation and ionic strength. *J King Saud Univ Eng Sci* 32(6): 351–359. https://doi.org/10.1016/j.jksues.2019.04.006
45. Tejada-Tovar C, Villabona-Ortíz Á, Gonzalez-Delgado ÁD. 2021. Adsorption of azo-anionic dyes in a solution using modified coconut (Cocos nucifera) mesocarp: kinetic and equilibrium study. *Water* 13(10): 1382. https://doi.org/10.3390/w13101382
46. Dandil S, Sahbaz DA, Acikgoz C. 2019. Equilibrium and kinetic studies of reactive black 8 adsorption onto crosslinked chitosan beads. *J Chem Chem Eng* 13: 1-7. https://doi.org/10.17265/1934-7375/2019.01.001
47. Naik BNK, Mehandi S. 2025. Heterosis and combining ability study for yield contributing traits in chickpea (Cicer arietinum L.). *J Food Chem Nanotechnol* 11(S1): S54–S58. https://doi.org/10.17756/jfcn.2025-s1-009
48. Ma CM, Hong GB, Wang YK. 2020. Performance evaluation and optimization of dyes removal using rice bran-based magnetic composite adsorbent. *Materials* 13(12): 2764. https://doi.org/10.3390/ma13122764
49. Gupta VK, Mittal A, Malviya A, Mittal J. 2009. Adsorption of carmoisine A from wastewater using waste materials--bottom ash and deoiled soya. *J Colloid Interface Sci* 335(1): 24–33. https://doi.org/10.1016/j.jcis.2009.03.056
50. Hamza W, Dammak N, Hadjltaief HB, Eloussaief M, Benzina M. 2018. Sono-assisted adsorption of cristal violet dye onto Tunisian smectite clay: characterization, kinetics and adsorption isotherms. *Ecotoxicol Environ Saf* 163: 365–371. https://doi.org/10.1016/j.ecoenv.2018.07.021
51. Rapo E, Posta K, Suciu M, Szép R, Tonk S. 2019. Adsorptive removal of Remazol brilliant violet-5R dye from aqueous solutions using calcined eggshell as biosorbent. *Acta Chim Slov* 66(3): 648-658. https://doi.org/10.17344/ACSI.2019.5079
52. Rápó E, Jakab K, Posta K, Suciu MA, Tonk SZ. 2020. A comparative study on the adsorption of two Remazol dyes on green adsorbent. *Rev Chim* 71(4): 248–257. https://doi.org/10.37358/rc.20.4.8063
53. Keshavarzi F, Samaei MR, Hashemi H, Azhdarpoor A, Mohammadpour A. 2024. Application of montmorillonite/octadecylamine nanoparticles in the removal of textile dye from aqueous solutions: modeling, kinetic, and equilibrium studies. *Heliyon* 10(14): 1-15. https://doi.org/10.1016/j.heliyon.2024.e25919
54. Liu Y, Gao H, Li Z, Han R. 2024. Magnetic bio-composite based on zirconium and chitosan modified activated carbon from peanut husk with enhanced antibacterial and adsorptive potential for alizarin red and congo red in wastewater. *Int J Biol Macromol* 273: 132995. https://doi.org/10.1016/j.ijbiomac.2024.132995
55. Han R, Zhang L, Song C, Zhang M, Zhu H, et al. 2010. Characterization of modified wheat straw, kinetic and equilibrium study about copper ion and methylene blue adsorption in batch mode. *Carbohydr Polym* 79(4): 1140–1149. https://doi.org/10.1016/j.carbpol.2009.10.054
56. Langmuir I. 1916. The constitution and fundamental properties of solids and liquids. Part I. Solids. *J Am Chem Soc* 38: 2221–2295.
57. Freundlich H. 1906. Surface influences on bler and beer preparation. *J Chem Indus Colloid* 1: 152. https://doi.org/10.1007/BF01813581
58. Saadi R, Saadi Z, Fazaeli R, Fard NE. 2015. Monolayer and multilayer adsorption isotherm models for sorption from aqueous media. *Korean J Chem Eng* 32(5): 787–799. https://doi.org/10.1007/s11814-015-0053-7
59. Liu Y, Shen L. 2008. From Langmuir kinetics to first- and second-order rate equations for adsorption. *Langmuir* 24(20): 11625–11630. https://doi.org/10.1021/la801839b
60. Wang H, Zhao L, Hou W. 2024. Pseudo-second-order kinetic equation for describing the effect of sorbent and sorbate concentrations. *Langmuir* 40(7): 3559–3568. https://doi.org/10.1021/acs.langmuir.3c03235
61. Filipkowska U. 2006. Adsorption and desorption of reactive dyes onto chitin and chitosan flakes and beads. *Adsorpt Sci Technol* 24(9): 781–795. https://doi.org/10.1260/026361706781388932
62. Jiang K, Wu B, Wang C, Ran Q. 2019. Ecotoxicological effects of metals with different concentrations and types on the morphological and physiological performance of wheat. *Ecotoxicol Environ Saf* 167: 345–353. https://doi.org/10.1016/j.ecoenv.2018.10.048
63. Abdulrasool M, Ruaa K, Mays A, ALsailawi HA, Mudhafar M, et al. 2021. Regeneration of chitosan-based adsorbents used in heavy metal adsorption. *J Life Sci* 15: 11–19. https://doi.org/10.17265/1934-7391/2021.01.002